Measurements of the muon flux produced by 10.6 GeV electrons in a beam dump

M. Battaglieri[b], M. Bondí[a,*], A. Celentano[b], M. De Napoli[a], R. De Vita[b], S. Fegan[e], L. Marsicano[b,c], G. Ottonello[b], F. Parodi[b], N. Randazzo[a], E.S. Smith[d], T. Whitlatch[d]

[a] *INFN - Sezione di Catania, Via S. Sofia 64, I-95125 Catania, Italy*
[b] *INFN - Sezione di Genova, Via Dodecaneso 33, I-16146 Genova, Italy*
[c] *Universitá degli Studi di Genova, Via Dodecaneso 33, I-16146 Genova, Italy*
[d] *Jefferson Lab, Newport News, VA 23606, USA*
[e] *George Washington University, Washington DC, 20052, USA*

Abstract

This paper presents the results of an experiment to assess the muon flux produced by the interaction of a 10.6 GeV electron beam with the Hall-A beam dump at Jefferson Lab (JLab). The goal was to benchmark Monte Carlo simulations that are an essential tool for estimating beam-related backgrounds in beam-dump experiments aimed at searching for rare events, such as the Beam Dump eXperiment (BDX) planned at JLab. Beam-produced muons were measured with a CsI(Tl) crystal sandwiched between a set of segmented plastic scintillators placed at two different distances from the dump: 25.7 m and 28.8 m. At each location the muon flux was sampled at different vertical positions with respect to the beam height. Data have been compared with detailed Monte Carlo simulations using FLUKA for the muon production in the dump and propagation to the detector, and GEANT4 to simulate the detector response. The good agreement between data and simulations, within the uncertainties of the soil composition and density, demonstrate the validity of our simulation tools to predict the beam-related muon background in electron beam-dump experiments at ~ 10 GeV.

Keywords: Light Dark Matter, Dark Photon, Beam-dump experiment, Muon

*Corresponding author
Email address: mariangela.bondi@ct.infn.it (M. Bondí)

1. Introduction

Background is usually the limiting factor in experiments searching for rare events. This is the case for Dark Matter (DM) searches in beam-dump experiments where a high intensity O(GeV) electron/proton beam is directed into a dump producing an overwhelming shower of Standard Model particles in addition to the rare DM particles of interest. While most of the radiation (gamma, electron/positron and neutron) is contained in the dump or degraded down to harmless energy levels, deep penetrating radiation, such as muons, propagate for long distances before depositing their energy far from the point of origin[1]. Monte Carlo simulations are used to find the best combination of shielding and analysis cuts to minimize such background. However, they need to be validated with actual measurements. In this work we present the results of a measurement performed downstream of the JLab Hall-A beam-dump to asses the muon background produced in the interaction of the CEBAF 10.6 GeV electron beam with the dump. Experimental results have been compared to simulations performed with FLUKA [1, 2] and GEANT4 [3] that include a realistic model of the dump, the surrounding materials and the detector response. This study is relevant for the Beam Dump eXperiment (BDX) planned at Jefferson Lab. BDX is an electron-beam thick-target experiment aimed to produce and detect light Dark Matter particles (MeV-GeV mass range), in the framework of the theoretical paradigm where DM is charged under a new U(1) symmetry whose interaction is mediated by a new light vector boson (a *heavy photon* or A', also called *dark photon*)[4]. The A' is expected to be produced in the interaction of the high power ($\sim$1 GW) electron beam with the Hall-A beam dump via $A'-strahlung$ processes [5] and e^+e^- annihilations [6]. The A' could then decay

[1] Neutrinos are copiously produced in the dump but due to the low interaction cross section, they deserve a separate discussion.

into forward-boosted DM particles (χ) that may interact with the BDX detector located ~ 25 m downstream of the dump. An electromagnetic calorimeter with $\sim$800 CsI(Tl) crystals will measure the EM shower produced by high-energy e^- produced by the scattering of a χ with atomic electrons. Two large-area plastic-scintillator veto systems and a massive passive shielding placed downstream of the dump will be used to reject high energy backgrounds that can mimic a DM signal, except for neutrinos. In order to benchmark Monte Carlo simulations, an on-site experimental campaign was performed to measure the muon flux in the present unshielded configuration at the location of the future BDX detector. The measurement used an electron beam with the proposed energy (10.6 GeV) and one third the current ($\sim 20\,\mu$A) expected in the BDX experiment. To our knowledge, together with a previous measurement performed at SLAC in the seventies [7], this is the only dedicated measurement of 10 GeV electron beam muon production on a thick target and subsequent propagation.

2. Experimental setup

The muon flux was measured at the expected location for the future BDX facility [4] [2]. A schematic view of the test locations is shown in Fig.1.

Two wells were dug in the positions marked as Well-1 and Well-2. Two vertical PVC pipes, 10-inch diameter and 10 m in length, were installed at two locations approximately 26 m and 29 m downstream of the beginning of the dump. The precise localization of the two wells with respect to the Hall-A beam dump was established by two independent surveys performed by JLab Facility and JLab Survey groups[8, 9].

Table 1 reports survey positions for each well. The top of the pipes protrude about 76 cm above a concrete pad, which was used to anchor the pipes. The pad was about 15 cm higher at the upstream end than at the downstream with

[2] The measurements presented in this paper were performed in the present unshielded configuration consisting only of dirt (see text), whereas in the future BDX experiment the passive shielding between dump and facility will be composed of iron and concrete.

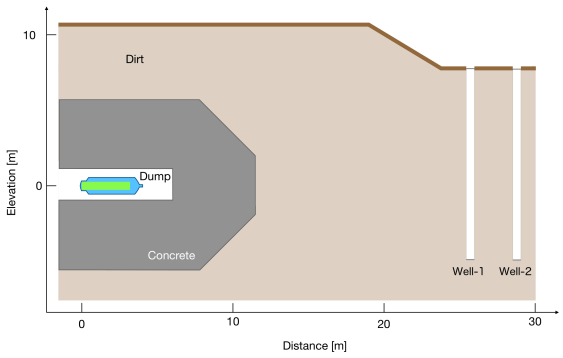

Figure 1: Schematic representation of the test locations. From left to right, the Hall-A aluminum-water beam dump (blue-green), the concrete beam-vault walls (gray), the dirt (brown), and the two vertical pipes. (Color online)

Item	Y(cm)	Z(cm)
Center of Hall A	0	0
Beginning of Beam Dump	0	5000
Center of Well 1 (beam height)	-1.3	7569
Center of Well 2 (beam height)	3.8	7874
Center of Well 1 (top flange)	0.6	7572
Center of Well 2 (top flange)	1.6	7879

Table 1: Location of the wells relative to the center of Hall A and the beam dump. The coordinate system uses Z along the beam line, and Y perpendicular to it pointing toward the north. Differences between the pipe centers at the top flange compared to beam height are indicators of how accurately the pipes could be placed and how vertical they stand.

a gradual step in between. The bottoms of the pipes were filled with about 122 cm of grout to prevent ground water from seeping inside. The bottom of pipe 1 was 155 cm below the beam line and the bottom of pipe 2 was 117 cm below the beam line.

The detector (see next section) was located inside a 20 cm diameter stainless-steel water-tight cylindrical vessel, shown in Fig. 3-B, covered by steel lids on top and bottom, supported by steel cables that were used to move it up and down using a hand winch. The electronic cable connections to the detector were routed through a 5 cm diameter PVC pipe that was firmly attached to the top of the vessel. The PVC pipe came in 6 of 122 cm sections that could be screwed together (or unscrewed) as the detector was hoisted up and down inside the well. The height of the detector was determined using a tape measure attached to the individual PVC segments with registration marks to ensure reproducibility as they were connected and disconnected. The location of the detector at beam height was checked by measuring a non-stretch fishing line lowered down with a plumb bob to the top of the vessel. The systematic error associated to the procedure was estimated to be $\Delta Y_{Pos} = \pm 5$ cm. Materials traversed by muons traveling from the dump to the detector are concrete (dump-vault) and soil. During the excavation, two soil samples were taken near the pipe locations resulting in $\rho_{dirt} = 1.93\,\mathrm{g/cm^3}$ and $1.95\,\mathrm{g/cm^3}$.

2.1. BDX-Hodo detector

The detector used to measure the muon flux, called the BDX-Hodo, is composed of a CsI(Tl) crystal sandwiched between a set of segmented plastic scintillators 1-2 cm thick. The detector has been designed using the same technology proposed for BDX in order to validate the technical choices in a realistic background environment, which is higher than the one expected in the BDX experiment [4, 10].

The crystal, formerly used in the BaBar Ecal [12], has a trapezoidal shape, with a $4.7 \times 4.7\,\mathrm{cm^2}$ and a $6 \times 6\,\mathrm{cm^2}$ small faces, ~ 31 cm in length. It is wrapped in a white, diffuse reflector material ($Tyvek$), then in aluminum foil, Mylar

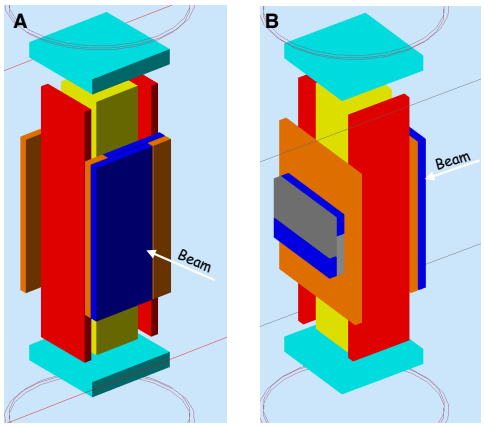

Figure 2: A GEMC-GEANT4 [11] implementation of the BDX-Hodo detector. Panel A and B show the front and back face of the detector, respectively. (Color online).

and black paper for light-proofing and insulation. Light is read by a $6\,\mathrm{x}\,6\,\mathrm{mm}^2$ Hamamatsu MPPC (S13360-6025PE) with a pixel pitch of $25\,\mu\mathrm{m}$, a photon detection efficiency of $\sim 22\%$ at 550 nm, corresponding to the maximum of the CsI(Tl) emission spectrum, and a gain of $7 \cdot 10^5$ at the nominal bias value and room temperature. The sensor is placed in the middle of the $4.7\,\mathrm{x}\,4.7\,\mathrm{cm}^2$ face optically coupled with optical grease. The bias voltage is provided by a custom-designed board, hosting a 5 V input tunable DC-DC converter [13]. The SiPM output signal is amplified by a trans-impedance amplifier with gain factor of 50.

The crystal side facing the beam dump is covered by four plastic scintillator paddles of different areas (two of $19.2\,\mathrm{x}\,8.0\,\mathrm{cm}^2$ and the others of $19.2\,\mathrm{x}\,2.5\,\mathrm{cm}^2$) arranged as shown in Fig. 2-A. One large-area ($19.2\,\mathrm{x}\,14.4\,\mathrm{cm}^2$) plastic scintillator paddle is located behind the crystal followed by four small-area paddles of different areas (two of $10.6\,\mathrm{x}\,5.0\,\mathrm{cm}^2$ and the others of $10.6\,\mathrm{x}\,2.5\,\mathrm{cm}^2$), arranged as shown in Fig. 2-B. Indeed, the requirement of a hit in both front and back paddles defines a $3\,\mathrm{x}\,3$ matrix of $2.5\,\mathrm{x}\,2.5\,\mathrm{cm}^2$ pixels providing cm-scale muon XY position resolution. Four more paddles covering the left/right sides ($31.4\,\mathrm{x}\,7.5\,\mathrm{cm}^2$) and the top/bottom ($11\,\mathrm{x}\,11\,\mathrm{cm}^2$) of the crystal are used to (partially) veto cosmic rays and other surrounding radiation not coming from

the beam direction. Light produced in the plastic scintillator was extracted by a wavelength-shifting fiber inserted into a $2\,\mathrm{x}\,2\,\mathrm{mm}^2$ groove on the paddle's surface and coupled to a $3\,\mathrm{x}\,3\,\mathrm{mm}^2$ Hamamatsu S12572-100 silicon photomultiplier (SiPM). A 3D-printed plastic mechanical support, shown in Fig. 3-A holds the detector components, including amplifier and bias voltage boards.

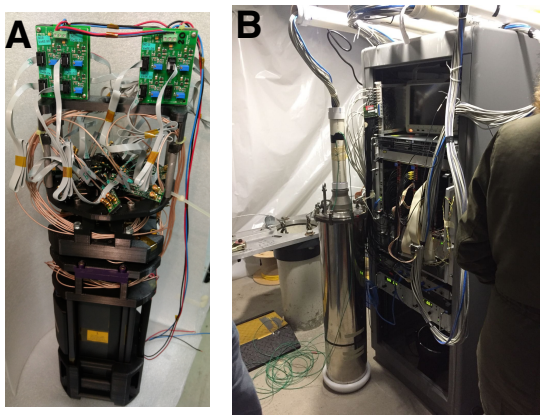

Figure 3: Some pictures of the detector assembled.

2.2. Data acquisition and trigger system

Each signal from the detector was sent to a 1:1 splitter, based on a passive resistor network. After splitting, one half of the signal was sent to a leading-edge discriminator (CAEN v895), while the other half was fed to a Flash Amplitude-to-Digital Converter (CAEN FADC v1725). The digital output from the discriminator was sent to a programmable logic board (CAEN FPGA v1495) implementing the trigger logic and generating the trigger signal for the FADC. All the readout boards were hosted in a VME64x crate. Thanks to the large plastic scintillators light yield and the high SiPM quantum efficiency, the energy deposition of passing-through minimum-ionizing particles resulted in very large signals at the preamplifier output: a threshold of 250 mV for the corresponding discriminator channels was used. On the other hand, for the CsI(Tl) crystal a low threshold of $\sim 5\,\mathrm{MeV}$ was implemented.

The v1725 FADC (250 MHz sampling frequency, 14 bits resolution, and 2 V maximum amplitude) digitized and stored input signals in an internal circular buffer. When a trigger was received, the digitized data within a programmable window was reported for readout without any further elaboration. We operated the FADC boards with a 630 samples (2.520 μs) readout window width, sufficiently large to record the full wave form of every signal. The position of the signal within the readout window was properly adjusted through an ad-hoc delay implemented in the trigger FPGA board.

Trigger #	**Definition**
0	Back-Large && (Front-1 || Front-2)
1	Top && Bottom
2	Left && Right
3	Crystal
4	50-Hz Pulser

Table 2: Summary of trigger bits implemented in the programmable logic board.

Various trigger equations were implemented through a custom firmware for the Cyclone EP1C20 FPGA hosted in the programmable logic board v1495. Table 2 reports the trigger bit definition. The global trigger signal is defined as the "OR" of all trigger bits. Each trigger bit featured an independent pre-scale factor, and the corresponding rate - before and after pre-scaling - was measured through a scaler counter implemented in the firmware. Pre-scale factors for trigger bits other than the main one (#0) were adjusted for each run to keep the overall DAQ live-time greater than 85%. Live-time information, as well as the trigger bit rates and pre-scale factors, were injected approximately every 3 s into the data stream and used in the off-line analysis to properly calculate the absolute event rate. The standard JLab "Cebaf Online Data Acquisition" (CODA) software was used to handle the readout system [14]. The VME crate hosted a Readout Controller (ROC) that, upon receiving a trigger, collected digitized data from the FADC, and sent them to the Event Builder (EB). The

EB assembles information from the boards into a single event, which was passed to the Event Recorder (ER), that finally wrote it to the disk. Data transferring from the EB to the ER was handled with the CODA Event Transfer system (ET-ring). The ET system provides a very fast and robust method of transferring events between different processes, running on different hosts on the same subnetwork. The Readout Controller was a XVR16 single board computer, featuring a multi-core Intel i7 processor, running the DAQ software on CentOs5 operating system. The EB, ER, and the other DAQ components, ran on a dedicated computer, with Scientific Linux 7 OS. The same machine also hosted the data storage.

3. Muon flux measurements

Measurements were performed using a 10.6 GeV electron beam with a steady current of 22 μA delivered by the CEBAF accelerator. A few special runs were taken at different beam currents: 2.2 μA, 5 μA, and 10 μA. During the test, the BDX-Hodo detector was lowered in the pipe and the muon flux sampled at different heights with respect to nominal beam height. The muon flux profiles in Y (vertical direction), measured at the two different locations in Z (distance from the dump), allowed us to compare the absolute and relative MC predictions.

3.1. Data reconstruction procedure

We adopted the following data-reconstruction procedure within the "JLab Data Analysis Framework"(JANA) [15]. First and foremost we excluded from the analysis those events corresponding to beam-trip time intervals identified by monitoring the crystal rate every second. We also excluded time bins where the measured crystal rate was below 30% of the mean rate for stable beam conditions. Moreover, the events collected 30 s after and before the beam-trip time interval were thrown away. As an example, the measured rate in the crystal as a function of time is reported in Fig. 4.

For the CsI(Tl) crystal, the signal waveform was numerically integrated within a 1 μs time window to obtain the corresponding charge. This was con-

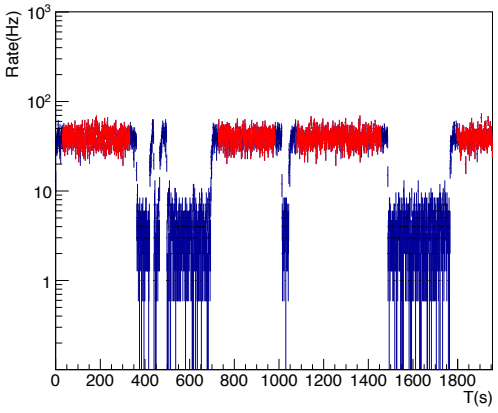

Figure 4: Example of rate measured in the crystal as a function of time. The rate going to zero corresponds to beam-trip events. The full data set is shown in blue. Only data acquired during stable beam-current conditions (red points) have been included in the data analysis. (Color online)

verted in MeV units by using calibration constants deduced from the deposited energy by the muons in the crystal, evaluated through Monte Carlo simulations.

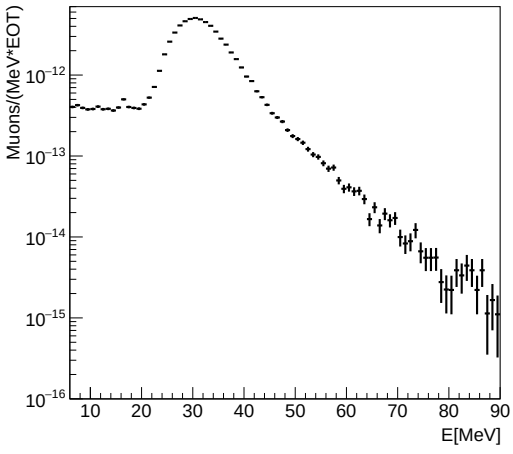

Figure 5: Measured event rate, in well-1 at beam height, normalized to the beam current as a function of deposited energy in the crystal requiring the 3-fold coincidence.

For plastic scintillator detectors, signals were first integrated in a 1 μs time window and the integral normalized to the single photo-electron charge recorded in dedicated pulser runs.

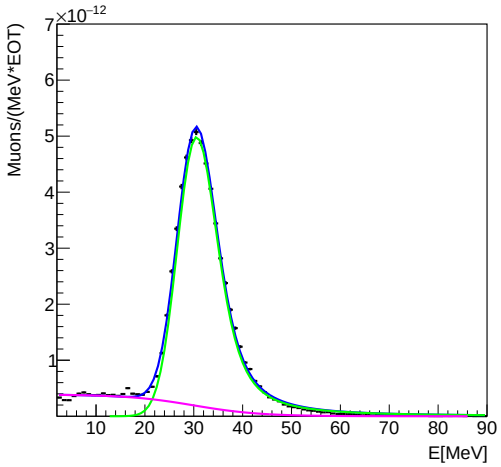

Figure 6: Example of a best fit (blue) to the CsI(Tl) crystal energy spectrum used to extract rate of beam-related minimum-ionizing muons crossing the crystal. The fit has been performed using a Landau function convoluted with a Gaussian (green) and a Fermi function (pink) to model the low-energy flat part.

In the off-line analysis, independently on the trigger bit, muons are selected by requiring a 3-fold coincidence between crystal, front and back scintillator paddles, resulting in an effective area of $\sim 5\,\mathrm{x}\,19.2\,\mathrm{cm}^2$. An example of the muon rate normalized to the number of electron on target (EOT) as a function of the deposited energy in the crystal is shown in Fig. 5. The crystal energy spectrum was fitted to a Landau function convoluted with a Gaussian, modeling the low-energy flat part with a Fermi function, as shown in Fig. 6. The rate of minimum-ionizing muons was obtained by integrating the Landau function from 0 to 120 MeV. The main source of uncertainty in the extracted rates is related to the Fermi function parametrization. It is included in error bars in all subsequent plots.

3.2. Experimental results

We first established the correlation between the beam current and the muon rate at a fixed detector position. Figure 7 shows the rate measured with the detector in Well-1 positioned at the nominal beam height for 4 different beam current values: 2.2 µA, 5 µA, 11 µA, and 22 µA. As expected, the muon rate dependence on current is linear.

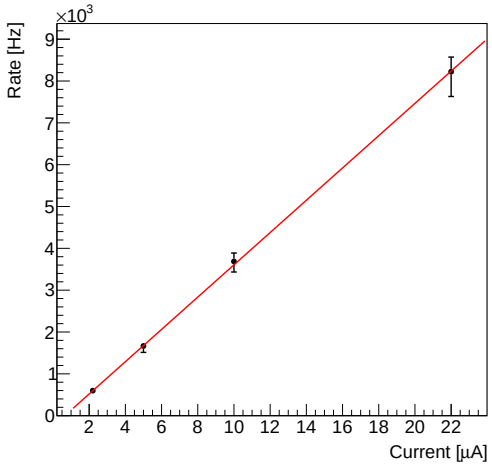

Figure 7: Muon rate measured inside the well-1 at the beam line height as a function of the beam current. The line is the linear best-fit of the data.

The muon fluxes sampled at different heights with respect to the beam-line for Well-1 and Well-2 are shown in Fig. 8. Positive (negative) position values refer to detector positions above (below) the beam-line. In the figures, the distributions have been shifted by -10 cm (Well-1) and -40 cm (Well-2) in order to approximately center the maximum rate at zero. A possible explanation for the observed shifts could be the presence of a non-uniform soil density profile between the dump and the detector, as a function of the vertical position. Indeed, simulations performed using a simplified linearly-changing density-profile are able to qualitatively reproduce the misalignment of the muon flux distributions in both wells.

The maximum rates measured in Well-1 and Well-2 were found to be 8.4 ± 1.3 kHz

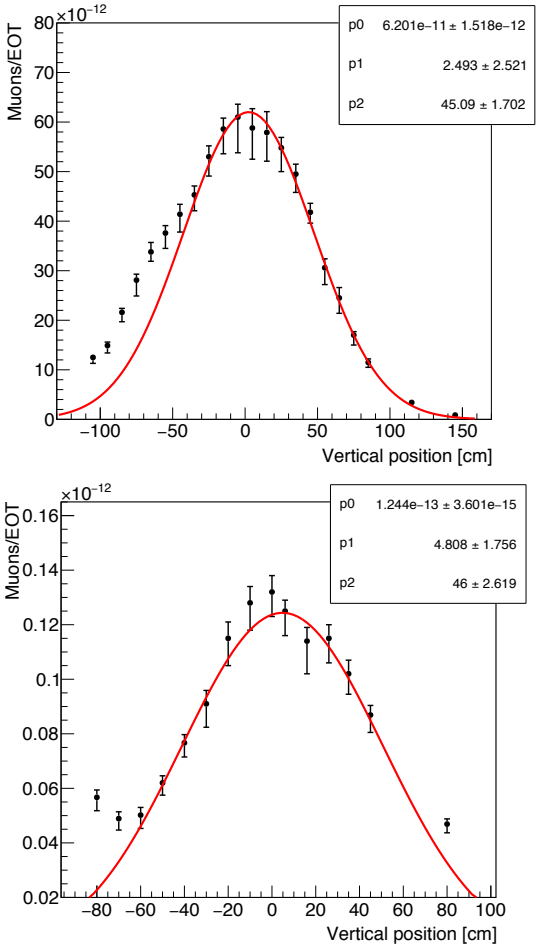

Figure 8: Muon rate as a function of the detector vertical position measured in Well-1 (Top panel) and Well-2 (bottom panel). The line is the Gaussian best-fit of the data.

and 17.7 ± 2.0 Hz, respectively. These rates can be converted into fluxes considering the detector cross-sectional area of $\sim$96 cm^2 and 22 μA beam current, resulting in fluxes of $\sim$4 Hz/(μA·cm^2) and $\sim 8.3 \cdot 10^{-3}$ Hz/(μA·cm^2) for Well-1 and Well-2, respectively. In deriving the muons flux from the measured rate on the detector, we made the assumption that particles are impinging on it with a negligible angle with respect to the normal direction. This assumption is justified by the geometry of the experimental setup, given the large distance between the target and the detector. It is worth noting that the muon rates drop by a factor $\sim$470 by moving the detector just 3 meters apart (along Z direction). This indicates the extreme sensitivity of the measured rate to the muon absorption by the traversed dirt showing that Well-2 is close to the edge of the muon range.

Detected rates as a function of the shift from the nominal beam height in the two wells show a nearly symmetric shape around the maximum. They were fitted to Gaussian functions finding a similar widths of $\sigma = (45 \pm 2)$ cm and $\sigma = (46 \pm 3)$ cm for Well-1 and Well-2, respectively. For both wells, data points in the range of -50 cm to -100 cm show an excess of counts above the fitted Gaussian. This may be due to variations, specifically a reduction, in the soil density traversed by incoming muons below the beam height.

3.3. Cosmic-ray background

In order to asses possible cosmic-muon backgrounds affecting the beam-related muon flux measurement, a dedicated beam-off cosmic run was performed deploying the detector in the Well-2 pipe at +30 cm with respect to the beam height. Fig. 9 shows the rate of cosmic events as a function of the deposited energy in the crystal obtained by applying the same cuts (no trigger bit selection and Front/Back paddles/Crystal three-fold coincidence) used to select the muons during beam tests.

The rate of minimum-ionizing events, extracted using the same fit procedure described for the beam-related data, is 0.08 ± 0.02 Hz. It is negligible when compared to measured beam-on muon rates (in all cases >10 Hz).

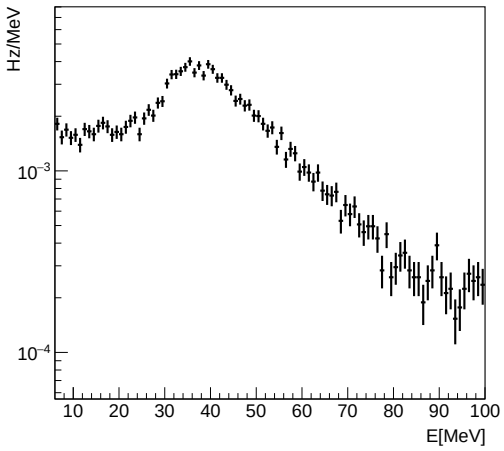

Figure 9: Rate of cosmic muons as a function of the energy deposited in the crystal when the Front/Back Paddles/Crystal three-fold coincidence is required.

4. Monte-Carlo simulations

We used a simulation framework based on FLUKA and GEANT4 in order to simulate the interaction of the 10.6 GeV electron-beam with the dump and the subsequent muon propagation from the dump to the BDX-Hodo detector. We used the existing configuration of the Hall-A beam dump geometry and materials implemented in FLUKA-2011.2c.5 by the Jefferson Lab Radiation Control Department [16]. The input card used to run the program includes all physics processes and a tuned set of biasing weights to speed up the running time while preserving accuracy. FLUKA was used to generate muons in the beam-dump and propagate them to a plane near the detector. From there, GEANT4 was used to track particles all the way up to the detector. The precise position of the two pipes, the composition of the shielding between the dump and pipes, as well as details of the beam parameters (current, energy) were included in the simulation. Geometry, materials and detector response were implemented in GEANT4 via the GEMC interface [11]. In particular the detailed description of the CsI(Tl) crystal response includes: a light yield (LY) of 50,000 Photons/MeV and a scintillating decay time of 800 ns (as measured by BaBar

Collaboration [12]), a Birks constant of $3.2{\cdot}10^{-3}\,\mathrm{g/(MeV{\cdot}cm^2)}$ [17], the charge collection spread induced by the finite crystals attenuation length of 53 cm, as reported in Ref. [18], and the SiPM nominal photon detection efficiency (PDE) at the wavelength corresponding to the maximum of the CsI(Tl) scintillation emission spectrum. Using these values it was possible to generate a realistic waveform (in photo-electron units) whose integral was compared to the measured waveform spectrum. Figure 10 shows the energy spectrum in the CsI(Tl) crystal, after selecting events with coincidence between crystal, front, and back plastic scintillator counters: data are shown as black circles while simulation results are shown as red squares. The absolute scale of each distribution was tuned to have the same normalization for deposited energy >10 MeV. The two distributions are in very good agreement, confirming the goodness of the crystal response parametrization in MC to passing-through muons.

The response of plastic scintillator paddles was implemented in the simulation in an effective way. The response in photoelectrons as well as the inefficiency to detect a crossing cosmic muon were measured for each paddle in dedicated tests before assembling the detector. On average, a MIP was found to have the most probable value of the associated Landau distribution in the range of 170-200 photo-electrons with a detection efficiency $> 98\%$. Since paddles were only used to tag muons, limiting the angular and the path-length spreads in the crystal, the parametrization implemented in the simulation was considered be accurate enough.

The composition and density of materials traversed by muons while traveling from the dump to the detector (beam-dump vault concrete walls and soil) are important parameters entering in the simulation. For the soil density we used a range of values around the ones sampled. We could not sample the concrete and therefore we assumed a nominal value for $\rho_{concrete}$ in the range $(2.2\text{ - }2.4)\,\mathrm{g/cm^3}$. Simulations show a significant dependence on density of traversed materials: Figure 11 shows that for a mere variation of 3% on ρ_{dirt} around $1.93\,\mathrm{g/cm^3}$ and 10% change in $\rho_{concrete}$ around $2.3\,\mathrm{g/cm^3}$, the rates in Well-1 and Well-2 vary by a factor $\sim$1.3 and $\sim$4, respectively. While the absolute value is

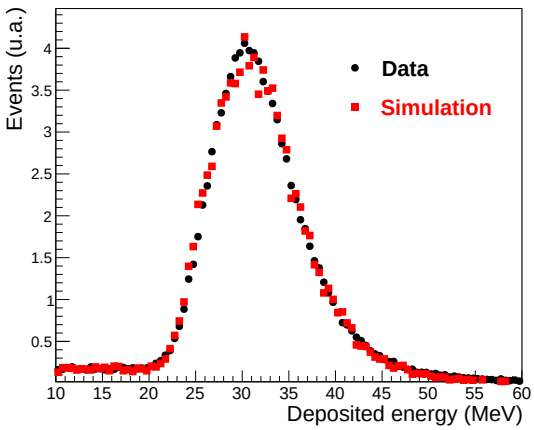

Figure 10: CsI(Tl) crystal energy spectrum for events with a coincidence between crystal, front and back plastic scintillator counters. Data are shown as black circles while red squares represents simulation results.

significantly affected, the shape of the distribution is less sensitive to the density variation. Detailed knowledge of the dirt/concrete density/uniformity along the muon flight path would require an effort beyond the scope of this work and therefore, to compare to the data, we ran simulations with the nominal value of $\rho_{dirt} = 1.93\,\mathrm{g/cm^3}$ and $\rho_{concrete} = 2.3\,\mathrm{g/cm^3}$ quoting the variation reported above as a systematic error band. Figure 12 shows the comparison of the measured and simulated rates as a function of the vertical height. Simulations, normalized to the beam current, agree to experimental data both on absolute values and shape of the rate profile. Remarkably, they are able to reproduce the suppression factor of $\sim$500 between rates measured in Well-1 and Well-2 as well as the gaussian shape and width.

We would like to stress that the limited knowledge of the dirt density in this test does not affect the simulation of the BDX experiment. These uncertainties are avoided in the the BDX set-up since we are planning to replace the current dirt with shielding materials with well-defined density and composition (most likely iron).

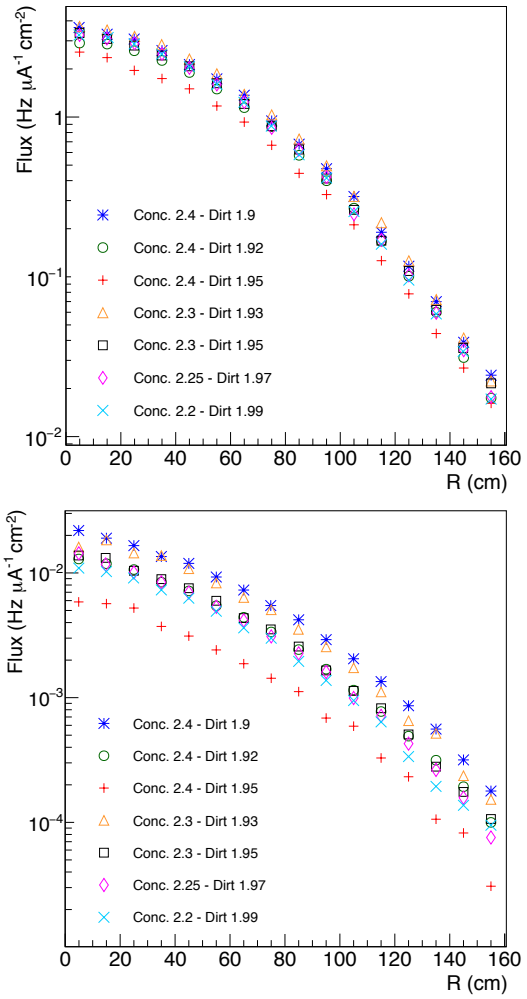

Figure 11: Simulated muon flux as a function of the sampling distance from the beam-height in Well-1 (top) and Well-2 (bottom). Sets of points correspond to different combination of ρ_{dirt} and $\rho_{concrete}$. Values quoted in the legend are expressed in g/cm^3.

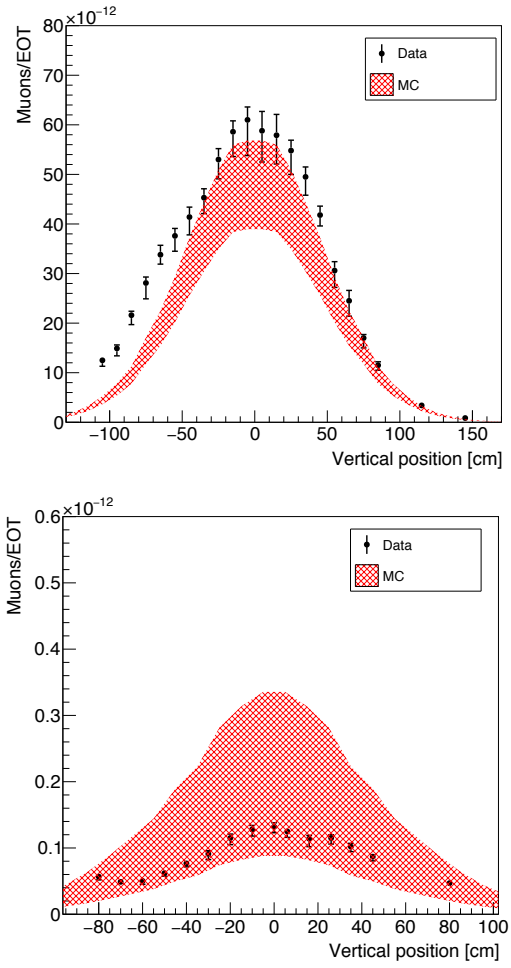

Figure 12: Comparison between simulated and measured muon rates. Well-1 (Well-2) is shown in the top (bottom) plot. The red error band include the systematic error related to the density uncertainty as explained in the text.

5. Conclusion

We measured the fluence of muons produced by interactions of 10.6 GeV electron beam with the JLab Hall-A beam-dump. The measurement, performed at ∼26 m and ∼29 m downstream of the beam-dump, provided the absolute muon rate at different vertical positions up to 1 m above and below beam height. The results show a significant drop in the muon rates between the two locations (from 8.4 kHz to 17 Hz) due to the proximity of the muon range. This variation implies a significant dependence on the traversed material composition and density, which calls for a precise assessment of the BDX shielding design. The measurements were compared to detailed FLUKA and GEANT4 simulations. The good agreement in absolute value and shape demonstrates that the simulation framework can safely be used to estimate the beam-related muon background in the BDX experimental set-up.

Acknowledgments

This material is based upon work supported by the U.S. Departmentof Energy, Office of Science, Office of Nuclear Physics under contract DE-AC05-06OR23177. The authors wish to thank: the INFN-CT, INFN-GE and JLab-Hall-D technical staff for the excellent work in constructing the detector and support during the measurement campaign, JLab Facilities for design, survey and logistical support, JLab Networking/Computing for providing connectivity, the JLab Hall-A for supporting the tests and allocating some beam time for the current scan, and finally Prof. William Wisniewski for providing the CsI(Tl) crystal.

References

[1] T. T. Bhlen, F. Cerutti, M. P. W. Chin, A. Fass, A. Ferrari, P. G. Ortega, A. Mairani, P. R. Sala, G. Smirnov, V. Vlachoudis, The FLUKA Code: Developments and Challenges for High Energy and Medical Applications, Nucl. Data Sheets 120 (2014) 211–214. doi:10.1016/j.nds.2014.07.049.

[2] A. Ferrari, P. R. Sala, A. Fasso, J. Ranft, FLUKA: A multi-particle transport code (Program version 2005).

[3] S. Agostinelli, et al., GEANT4: A Simulation toolkit, Nucl. Instrum. Meth. A506 (2003) 250–303. doi:10.1016/S0168-9002(03)01368-8.

[4] M. Battaglieri, et al. (BDX collaboration), Dark matter search in a Beam-Dump eXperiment (BDX) at Jefferson Lab, arXiv:1607.01390 [hep-ex].

[5] E. Izaguirre, G. Krnjaic, P. Schuster, N. Toro, New electron beam-dump experiments to search for mev to few-gev dark matter, Phys. Rev. D 88 (2013) 114015.

[6] L. Marsicano, et al., Novel way to search for light dark matter in lepton beam-dump experiments, Phys. Rev. Lett. 121 (2018) 041802. doi:10.1103/PhysRevLett.121.041802.

[7] W. R. Nelson, K. R. Kase, G. K. Svensson, Muon shielding around high-energy electron accelerators, Nucl. Instrum. Meth. 120 (1974) 056009.

[8] T. Whitlatch, S. Chandra, K. Trembly, private communication, 2018.

[9] E. Winslow, C. Curtis, T. Michalski, private communication, 2018.

[10] M. Bondí, Light dark matter search in a beam-dump experiment: Bdx at jefferson lab, EPJ Web Conf. 142 (2017) 01005.

[11] M. Ungaro, Clas12 geant4 simulation package gemc (2016).
URL http://gemc.jlab.org.

[12] B. Aubert, et al., The Babar detector, Nucl. Instr. Methods A 479 (2002) 1.

[13] A. Celentano, et al., The High Voltage Regulator Board for the BDX Experiment, Tech. rep., INFN-17-03/GE (2017).

[14] JLab CODA (2018).
URL https://coda.jlab.org/drupal/

[15] D. Lawrence, Multi-threaded event reconstruction with jana, Journal of Physics: Conference Series 119 (2008) 042018.

[16] M. Kharashvili, Jlab-tn-16-048, Tech. rep. (2016).

[17] V. I. Tretyak, Semi-empirical calculation of quenching factors for ions in scintillators, Astroparticle Physics 33 (2010) 40.

[18] M. Bondí, M. Battaglieri, M. Carpinelli, A. Celentano, M. De Napoli, R. De Vita, L. Marsicano, N. Randazzo, V. Sipala, E. S. Smith, Large-size CsI(Tl) crystal read-out by SiPM for low-energy charged-particles detection, Nucl. Instrum. Meth. A867 (2017) 148–153. doi:10.1016/j.nima.2017.06.024.